Medicinal Chemistry Research (2019) 28:696–710
https://doi.org/10.1007/s00044-019-02328-2

MEDICINAL CHEMISTRY RESEARCH

ORIGINAL RESEARCH

First report of antioxidative abeo-oleanenes from red seaweed *Gracilaria salicornia* as dual inhibitors of starch digestive enzymes

Kajal Chakraborty[1] · Tima Antony[1,2]

Received: 20 November 2018 / Accepted: 13 March 2019 / Published online: 24 March 2019

Abstract

Carbolytic enzyme-associated cascades have been considered as potential curative target in attenuating diabetic mellitus pathogenesis. Two oleanene class of triterpenoids characterised as 24(4 → 23), 27(8 → 26), 30(20 → 29)-tris-abeo-olean-(12-oxo)-1,15,22-triene-methyl hept-5-enoate (**1**) and 24(4 → 23)-abeo-olean-(12-oxo)-3,5-diene-deconoate (**2**) with potential inhibitory activities against the starch digestive enzymes α-glucosidase and α-amylase, were purified from the organic extract of intertidal red seaweed *Gracilaria salicornia* (family Gracilariaceae). Structural interpretation of compounds was carried out by detailed spectroscopic analysis, and their antioxidant/anti-diabetic potentials were assessed. Inhibitory potential of abeo-oleanene derivative (**2**) towards the starch digestive enzymes, α-glucosidase (IC_{50} 0.29 mM) and α-amylase (IC_{50} 0.32 mM) were greater than those displayed by its abeo-oleanene chemotype **1** (IC_{50} 0.34–0.40 mM). The molecular modelling studies were performed to designate the α-amylase and α-glucosidase inhibitory mechanism of oleanene analogues, and the comparison of docking parameters suggested that compound **2** exhibited least binding energy of −10.04 and −9.84 kcal mol^{-1} towards α-amylase and α-glucosidase respectively, and those results were corroborated with its greater inhibition potential against carbolytic enzymes. These results demonstrated that abeo-oleanene derivative (**2**) might constitute prospective anti-hyperglycaemic pharmaceutical candidate to moderate the likelihood of type-II diabetes.

Keywords *Gracilaria salicornia* · Gracilariaceae · Abeo-oleanenes · Anti-diabetic · Starch digestive enzymes · Biosynthetic pathway

Introduction

The onset and progress of diabetic pathogenesis is associated with disrupted glucose homoeostasis and resulting in cellular imbalance of carbohydrate and lipid metabolism (Henriksen et al. 2011). This disrupted functioning is instrumental in the progression to elevated postprandial blood glucose levels. The hydrolysis of starch by pancreatic α-amylase and absorption of glucose by intestinal α-glucosidases are responsible for this abrupt rise in blood glucose levels in hyperglycaemic conditions. Hence, the inhibition of pancreatic α-amylase and intestinal α-glucosidases was considered as an effective strategy for diabetic mellitus management (Kwon et al. 2007). However, the mild α-amylase inhibitors attracted more attention due to the improper bacterial fermentation of carbohydrates by concentrated α-amylase inhibitors (Kumar et al. 2011). Even though, numerous anti-diabetic strategies concentrate on increasing production and sensitivity of insulin, and/or reducing the blood glucose level. Newer α-amylase and α-glucosidase inhibitors, which can effectively maintain the cellular balance of carbohydrate and lipid metabolism associated with prevalence of diabetic mellitus, are being studied (Tahrani et al. 2011). Owing to the various adverse effects of synthetic drugs towards hyperglycaemia, naturally derived inhibitors have gained significant role in the modern health management (Nazaruk and Borzym-Kluczyk 2015).

These authors contributed equally: Kajal Chakraborty, Tima Antony

Supplementary information The online version of this article (https://doi.org/10.1007/s00044-019-02328-2) contains supplementary material, which is available to authorised users.

✉ Kajal Chakraborty
kajal_cmfri@yahoo.com
kajal.chakraborty@icar.gov.in

[1] Marine Bioprospecting Section of Marine Biotechnology Division, Central Marine Fisheries Research Institute, Ernakulam North, P. B. No. 1603, Cochin, India

[2] Department of Chemistry, Mangalore University, Mangalagangothri- 574199, Mangaluru, Karnataka, India

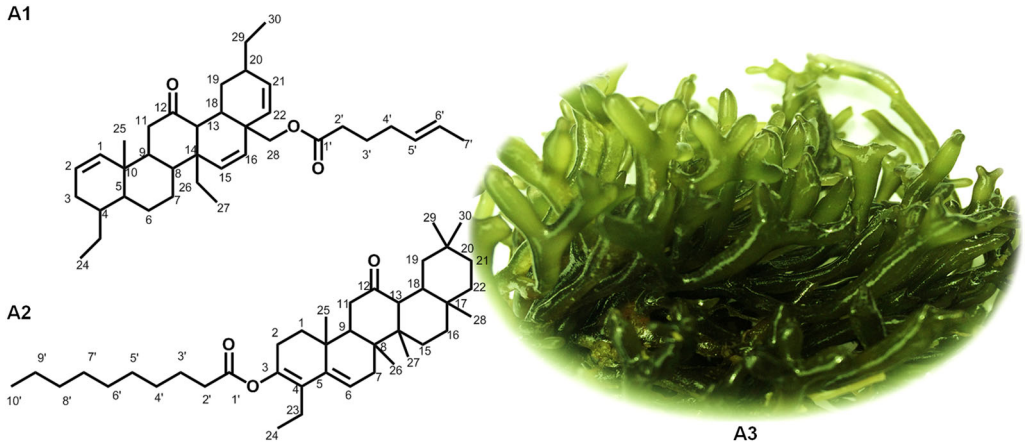

Fig. 1 Structural representations of (**A1**) 24(4 → 23), 27(8 → 26), 30 (20 → 29)-tris-abeo-olean-(12-oxo)-1,15,22-triene-methyl hept-5-enoate (**1**) and (**A2**) 24(4 → 23)-abeo-olean-(12-oxo)-3,5-diene-deconoate (**2**) isolated from *G. salicornia*. (**A3**) Representative photograph of thalli of the red seaweed *G. salicornia*

Seaweeds are marine natural sources, which were endowed with pharmaceutical potentials due to the occurrence of bioactive compounds belonging to various classes of chemistries (Antony and Chakraborty 2018; Maneesh and Chakraborty 2017). They were reported to hinder the function of carbolytic enzyme-associated cascades in glucose metabolism and normalise the change in insulin and plasma glucose levels. Among different bioactive compounds, triterpenoids, which constitute a wide range of biogenetically derived structurally divergent class of natural compounds resulting from thirty-carbon squalene or analogues precursors, were found to possess potential anti-hyperglycaemic properties (Nazaruk and Borzym-Kluczyk 2015; Hill and Connolly 2012). Most of these compounds are tetracycles (6-6-6-5), pentacycles {6-6-6-6-5(6)}, although mono-, bi-, tri-, hexacyclic and acyclic class of triterpenoids were identified from naturally occurring resources (Ruzicka 1963). Triterpenoids are ubiquitous in marine organisms, such as in seaweeds (Cen-Pacheco et al. 2010), and more than 20,000 triterpenoid metabolites and their variants belonging to oleanane, ursane, lanostane, dammarane, lupane, hopane, along with their pharmacological potential, were characterised (Hill and Connolly 2012; Laszczyk 2009). Pentacyclic oleanene triterpenoids derived from natural sources were found to be pharmacologically active compounds that were found to lessen the likelihood of postprandial hyperglycaemia by obstructing the functionalities of starch digestive enzymes (Lee et al. 2017). Oleanane triterpenoids with anti-diabetic properties were characterised from *Sambucus adnata* (Sasaki et al. 2011) and *Astilbe koreana* (Na et al. 2006). The inhibitory potencies of frido-oleanene triterpenoids against α-amylase and α-glucosidase were previously reported from the seaweed *Sargassum wightii* (Maneesh and Chakraborty 2017). Although these class of secondary metabolites deserve special consideration because of their targeted therapeutic potentials, very few studies were reported with the anti-diabetic activities of naturally derived triterpenoids (Nazaruk and Borzym-Kluczyk 2015).

The seaweed belonging to *Gracilaria sp* (Rhodophyceae) was found to attenuate potential antioxidant and anti-hyperglycaemia related pathogenesis (De Almeida et al. 2011; Sekar et al. 2015). *Gracilaria* sp are abundantly available in the coastal peninsular India with more than 300 reported species, and were recognised in industrial biotechnology due to the commercial product phycocolloid widely used in food, pharmaceutical and cosmetic industries (Francavilla et al. 2013). Among different species of the genus *Gracilaria*, *Gracilaria salicornia* (C. Agardh) E.Y. Dawson (family Gracilariaceae) was found to be ubiquitous in the coastal waters of Indian peninsular, and the species was not extensively studied to characterise the bioactive leads. This present study reported the purification and characterisation of two previously unreported triterpenoids of oleanane class of chemistries from the ethyl acetate-methanol (EtOAc-MeOH) extract of *G. salicornia* collected from the southeast coastal region of Indian peninsular. The studied compounds were designated as 24(4 → 23), 27(8 → 26), 30(20 → 29)-tris-abeo-olean-(12-oxo)-1,15,22-triene-methyl hept-5-enoate (**1**) and 24(4 → 23)-abeo-olean-(12-oxo)-3,5-diene-deconoate (**2**) (Fig. 1) by extensive spectroscopic experiments. The work also sought to examine the inhibitory potentials of the studied oleanane triterpenoids on key carbolytic enzyme related to diabetic mellitus (α-amylase and α-glucosidase) along with their antioxidant activities. The physicochemical descriptor variables were utilised to corroborate the structural attributes of the studied compounds with their bioactive potentials. In silico molecular

modelling studies were performed to designate the α-amylase and α-glucosidase inhibitory mechanisms of the studied oleanene analogues.

Materials and methods

General

Fourier transform infrared (FTIR) absorption spectra of the abeo-oleanene analogues were documented between 400–4000 cm^{-1} using potassium bromide (KBr) pellets on Perkin-Elmer FTIR Series 2000 spectrophotometer. An ultraviolet-visible spectrophotometer (Cary 50, Varian Cary, USA) was utilised for UV spectral analysis. The spectroscopic analysis including one-dimensional (^{1}H, 500 MHz; ^{13}C, 125 MHz; $^{135}DEPT$) along with two-dimensional NMR (HSQC, ^{1}H-^{1}H COSY, HMBC, NOESY) were carried out with a NMR spectrometer (Bruker Avance DPX, 500 MHz) using deuterated trichloromethane (Maneesh and Chakraborty 2017). A gas chromatograph-mass spectrometer (GC-MS) operating with the electron-impact (EI) mode (Varian GC model, CP-3800 housed in a mass spectrometer model Varian 1200 L) was used for the mass spectral analysis. The HPLC separations were carried out on a bonded-phase column (C_{18} reverse phase, 0.25 m × 0.46 cm, 5 µm, Phenomenex, USA), and the traces were detected with a diode-array detector (SPD M20A, Japan). A rotary evaporator (Heidolf, Germany) was used for removal of the solvents. The flash chromatographic instrument (Biotage-SP1, Sweden) mounting a silica gel (230–400 mesh, 12 g) column was used for purification. All spectroscopic and analytical-grade reagents and solvents were procured from Merck (Darmstadt, Germany).

Seaweed materials and extraction

The fresh samples of seaweed *G. salicornia* were obtained from Mandapam region (Gulf-of-Mannar, situated between 8°48′ N, 78°9’ E and 9°14’ N, 79°14’ E) of the peninsular India by scuba diving. The thalli of seaweed (voucher specimen number AC.3.1.1.4) were subjected to repeated washing with running water before shade-drying (for 3–4 days) at room temperature. The dried seaweed thalli were ground (1×10^3 g), and were extracted with equi-proportional volume (1:1 v/v, 500 mL) of ethyl acetate (EtOAc) and methanol (MeOH) at 55–60 °C for 4 h. The extracts were subjected for filtration (over filter paper Whatman No. 1) by sodium sulfate (125 g), and vacuum concentrated with a rotary evaporator (50 °C) for obtaining crude solvent mass (35 g) of *G. salicornia*. The filtrates were combined and vacuum concentrated at 55 °C using rotary evaporator (Heidolph, Instruments GmbH & Co., Schwabach, Germany) to one-fourth volume (Maneesh and Chakraborty 2017). The crude was subjected to chromatographic fractionation.

Chromatographic purification

The crude extract of *G. salicornia* (33 g) was fractionated by chromatographic separation techniques. Initially, a slurry of the crude was made with adsorbent silica gel (mesh size 60–120, 4 g), and was charged into the open glass column (100 cm × 4 cm) for fractionation. The separation of compounds was carried out with solvents of increasing polarity (100% *n*-hexane; EtOAc; MeOH) to collect forty-five fractions. The fractions (15 mL) were combined to eleven sub-fractions, which were referred to as TA_1-TA_{11} after TLC (*n*-hexane:EtOAc, 9:1 v/v) along with RP-C_{18}-HPLC (MeOH/acetonitrile (MeCN), 2:1 v/v) experiments. The pooled homogeneous fractions were assessed for their bioactive potencies, and the fractions with greater bioactive potential were subjected to further downstream purification. The column sub-fractions TA_2 (eluted after EtOAc:*n*-hexane, 1:4 v/v; 9.8 g, 29% yield) displayed free radical (DPPH and $ABTS^{+}$) scavenging potentials, and thus, subjected to further chromatographic separations. The fraction TA_2 was further fractionated over a silica gel column (45 cm × 3 cm, 230–400 mesh) using *n*-hexane/EtOAc (99:1 to 3:2 v/v) to yield twenty column fractions (32 mL each) that were combined to six fractions ($TA_{2\text{-}1}$-$TA_{2\text{-}6}$) on the basis of TLC (*n*-hexane:EtOAc, 9:1 v/v), as well as RP-C_{18} HPLC (MeOH/MeCN, 3:2 v/v). The column fraction, $TA_{2\text{-}1}$ (1.25 g), which was eluted with *n*-hexane:EtOAc (9:1 v/v) disclosed prospective scavenging activity towards DPPH radical. Therefore, $TA_{2\text{-}1}$ was further flash-fractionated (Biotage-SP1, Sweden) on adsorbent silica (230–400 mesh) with gradient elution of *n*-hexane/EtOAc (99:1 to 1:19, v/v) to acquire twelve fractions (10 mL each) that were combined to three fractions ($TA_{2\text{-}1\text{-}1}$ to $TA_{2\text{-}1\text{-}3}$) based on TLC (*n*-hexane:EtOAc, 9:1 v/v) and RP-C_{18} HPLC (MeOH/MeCN, 3:2 v/v). The column fraction $TA_{2\text{-}1\text{-}2}$ was subjected to preparatory RP-C_{18} HPLC purification (MeOH/MeCN, 2:1 v/v) to yield the compounds, **1** and **2** (98 and 102 mg, respectively), which were homogeneous after TLC (EtOAc:*n*-hexane, 1:19 v/v) and RP-C_{18} HPLC (MeCN/MeOH, 1:2 v/v).

Spectroscopic analysis

24(4 → 23), 27(8 → 26), 30(20 → 29)-Tris-abeo-olean-(12-oxo)-1,15,22-triene-methyl hept-5-enoate (1)

Pale yellow oily; UV_{MeOH} λ_{max} (log ε): 244 (2.91) nm (Fig. S1); TLC {silica-GF(254); EtOAc/*n*-hexane, 1:19 v/v} R_f: 0.38; R_t (RP-C_{18} HPLC, MeOH/MeCN 2:1, v/v): 3.41

min (Fig. S2); FTIR thin film (KBr) ν_{max} (bending δ, stretching ν, rocking ρ): 2930 (C-H_ν), 1730 {(-C(=O)-O-)$_\nu$}, 1726 (C=O_ν), 1458 (C=C_ν), 1406 (C-H_δ), 1238 (C-H_ρ), 1069 (C-C_ν), 723 (C-H_δ); cm^{-1} (Fig. S3). ^{1}H NMR, ^{13}C NMR, ^{135}DEPT, COSY, HSQC, HMBC and NOESY data (Table 1, Fig. S4–S10, Table S1); EI-MS *m/z*: calcd. for $C_{37}H_{54}O_3$ 546.4073, found 546.4076 $[M]^+$ (Δ 0.5 ppm) (Fig. S11–S12).

24(4 → 23)-Abeo-olean-(12-oxo)-3,5-diene-deconoate (2)

Yellowish oily; UV_{MeOH} λ_{max} (log ε): 247.24 (2.92) nm (Fig. S13); TLC {silica-GF(254); EtOAc /*n*-hexane, 1:19 v/v} R_f: 0.40; R_t (RP-C_{18} HPLC, MeOH:MeCN 2:1, v/v): 2.91 min (Fig. S14); FTIR thin film (KBr) ν_{max}: 2924 (C-H_ν), 1734 {(-C(=O)-O-)$_\nu$}, 1634 (C-O_ν), 1546 (C=C_ν), 1463, 1356 (C-H_δ), 1109 (C-C_ν), 722 (C-H_δ) (Fig. S15); ^{1}H NMR, ^{13}C NMR, ^{135}DEPT, COSY, HSQC, HMBC and NOESY data (Table 1, Fig. S16–S22, Table S2); EI-MS *m/z*: calcd. for $C_{40}H_{64}O_3$ 592.2485, found 592.2488 $[M]^+$ (Δ 0.5 ppm) (Fig. S23–S24).

Anti-diabetic and antioxidant activities

Anti-diabetic properties of the studied triterpenoids were evaluated by the inhibitory properties against α-amylase (source, porcine pancreas) and α-glucosidase (source, yeast) enzymes (Hamdan and Afifi 2004). Antioxidant potentials were analysed by 2,2′-azino-bis-3-ethylbenzothiozoline-6-sulfonic acid ($ABTS^+$) and 1,1-diphenyl-2-picryl-hydrazil (DPPH) (Wojdylo et al. 2007) radical assays. The results were indicated as IC_{50} (median inhibition concentration) values, which were obtained from the graph laid with sample concentration vis-à-vis percentage inhibition by enzymes/radicals in mM. The structure-activity correlation studies were carried out by utilising various structural descriptors (ACD Chemsketch ver-8.0; Chem Draw Ultra ver-8.0), such as partition coefficient of octanol-water (hydrophobic, log P_{ow}); electronic descriptor variable (polarisability, Pl); and steric (molar volume, MV; parachor, P; molar refractivity, MR).

In silico molecular modelling

Molecular modelling of the studied abeo-oleanenes were carried out using AutoDock-4 (ver-1.5.6). These titled compounds were constructed by ACD/ChemSketch (ver-2016.2.2, Toronto, Canada) and converted as MDL-Mol files that were saved as PDB format (Open Babel). X-ray crystal structures of α-glucosidase (PDB 3A4A; 1.6 Å) and α-amylase (PDB 1HNY; 1.8 Å) was retrieved from the Protein Data Bank (Brayer et al. 1995; Yamamoto et al. 2010) and conformationally arranged (Swiss-Pdb Viewer, ver-4.1.0). The molecular modelling analysis was carried out using Lamarckian algorithm methods, whereas the docking algorithm was run by Cygwin I-II. Following the completion of auto docking, the atomic positions RMSD (root-mean-square deviation) were examined, wherein the docking scores and binding energies were used to rank the preferred docked conformations. USCF Chimera (University of California, San Francisco, ver-1.11.2) software was used to visualise the molecular docking analyses.

Statistical analysis

The results were tabulated in triplicates with mean ± standard deviation. Significant differences ($P \le 0.05$) among the means were reported by using one-way variance analysis (Statistical Program for Social Sciences, USA, ver-13.0).

Results and discussion

General

Diabetes is one of the predominant diseases with high prevalence throughout the world, and the continued life with hyperglycaemic conditions leads to several glycated responses in our body (Perera et al. 2013). Consequently, pathophysiologies of hyperglycaemic conditions and identification of selective and targeted diabetic inhibitors to minimise the complications of this disease are the major subject area of research in medicinal chemistry (Wu et al. 2011). The abilities of various seaweed-derived metabolites that could hinder the carbolytic enzymes involved in the pathogenesis of diabetes were reported (Maneesh and Chakraborty 2017). The oleanene triterpenoid metabolites from seaweeds were found to be the prominent marine natural products with potential anti-diabetic properties (Da Rocha et al. 2015; Huang et al. 2013; Nazaruk and Borzym-Kluczyk 2015). There were accounts of similar classes of frido-oleanene compounds from seaweeds (Maneesh and Chakraborty 2017), including 3-(stearyloxy) olean-12-ene (Da Rocha et al. 2015), oleanane ester analogues, aceriphyllic acids from *Aceriphyllum rossii* and oleanane acetates from *Camellia japonica* (Hill and Connolly 2012). Consequently, the present study has been focused to isolate and characterise the rearranged triterpenes of oleanene class of chemistries from *G. salicornia* and to evaluate their antioxidative and anti-diabetic properties.

Bioassay-directed chromatographic purification of secondary metabolites of *G. salicornia*

Initial chromatography-assisted fractionation of EtOAc: MeOH crude extract of red seaweed, *G. salicornia* over

Table 1 NMR spectroscopic data[a] of abeo-oleanane type triterpenes (**1–2**) isolated from red seaweed *G. salicornia*

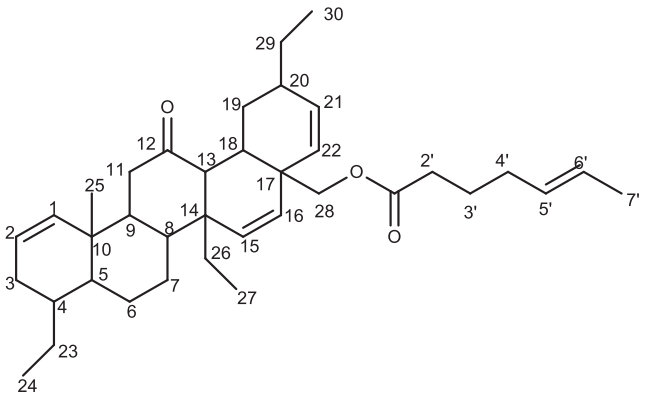

1

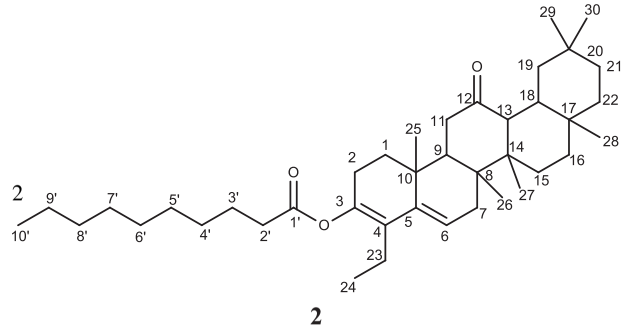

2

1

Type	C. No.	^{13}C NMR	^{1}H. No. (int., mult., *J* in Hz)[b]	^{1}H NMR	COSY	HMBC
CH	1	130.2	1H, *d*, *J* = 10.3 Hz	5.32	—	C-2,10
CH	2	127.8	1H, *dt*, *J* = 8.9, 7.6 Hz	5.28	H-3	—
CH_2	3	31.8	1H, *t*, *J* = 4.9 Hz	1.77	H-4	C-23
			1H, *t*, *J* = 4.9 Hz	2.01	—	—
CH	4	33.9	1H, *m*	1.62	H-5	C-24
CH	5	52.3	1H, *m*	1.30	H-6	C-23,9,10
CH_2	6	29.0	1H, *m*	1.51	H-7	C-5
			1H, *m*	1.28	—	—
CH_2	7	28.9	1H, *m*	1.55	H-8	—
			1H, *m*	1.26	—	—
CH	8	29.7	1H, *td*, *J* = 6.8, 5.2 Hz	1.33	H-9	C-13
CH	9	47.9	1H, *td*, *J* = 5.8, 5.5 Hz	1.66	H-11	C-12,25
C	10	46.8	—	—	—	—
CH_2	11	39.3	1H, *d*, *J* = 8.6 Hz	2.22	—	C-12
			1H, *d*, *J* = 8.0 Hz	2.27	—	—
C	12	193.7	—	—	—	—
CH	13	56.7	1H, *d*, *J* = 6.7 Hz	2.75	—	C-12,14,18
C	14	34.4	—	—	—	—

Type	C. No.	^{13}C NMR	^{1}H. No. (int., mult., *J* in Hz)[b]	^{1}H NMR	COSY	HMBC
CH_2	1	30.5	1H, *dt*, *J* = 13.0, 6.5 Hz	1.42	H-2	C-10, 5
			1H, *dt*, *J* = 13.9, 5.9 Hz	1.15	—	—
CH_2	2	24.7	1H, *dt*, *J* = 11.8, 7.8 Hz	2.03	—	C-1,3,4,1′
			1H, *dt*, *J* = 11.2, 6.2 Hz	1.72	—	—
C	3	132.2	—	—	—	—
C	4	128.8	—	—	—	—
C	5	139.2	—	—	—	—
CH	6	130.9	1H, *dd*, *J* = 6.8,13.2 Hz	5.82	—	C-5,7
CH_2	7	34.0	1H, *d*, *J* = 8.2 Hz	2.00	—	C-8
			1H, d, *J* = 5.0 Hz	1.75	—	—
C	8	42.7	—	—	—	—
CH	9	43.4	1H, *t*, *J* = 7.2 Hz	1.70	H-11	C-8,10,11
C	10	31.4	—	—	—	—
CH_2	11	36.9	1H, *dd*, *J* = 10.8, 3.2 Hz	2.33	—	C-12
			1H, *dd*, *J* = 9.9, 2.6 Hz	2.07	—	—
C	12	213.1	—	—	—	—
CH	13	51.9	1H, *d*, *J* = 12.9 Hz	2.30	H-18	C-12,8,14
C	14	38.8	—	—	—	—

Table 1 (continued)

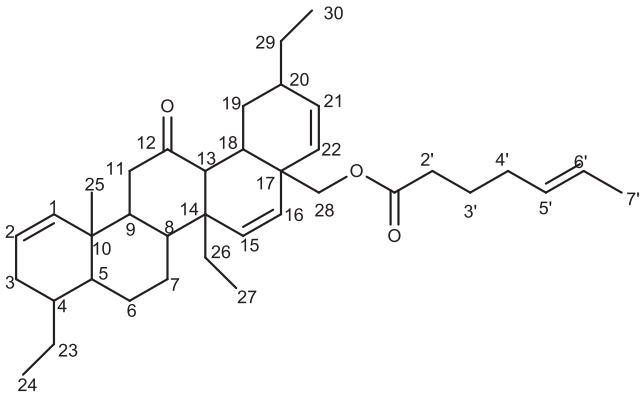

1

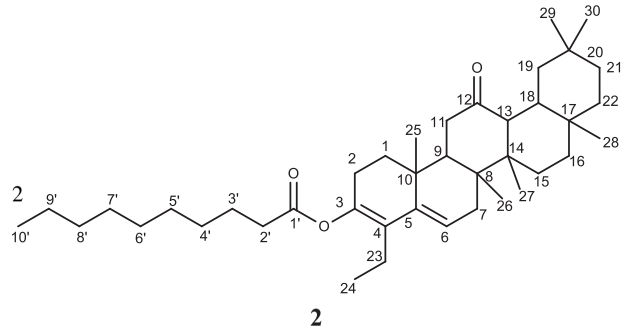

2

1

Type	C. No.	^{13}C NMR	^{1}H. No. (int., mult., *J* in Hz)[b]	^{1}H NMR	COSY	HMBC
CH	15	130.5	1H, *d*, *J* = 12.1 Hz	5.34	—	C-14
CH	16	127.7	1H, *d*, *J* = 13.0 Hz	5.30	—	C-15,17,28
C	17	43.5	—	—	—	—
CH	18	31.9	1H, *m*	2.77	—	C-19,17
CH_2	19	31.7	1H, *m*	1.65	H-20	—
			1H, *m*	1.56	—	—
CH	20	37.2	1H, *m*	1.93	H-21	C-29,22
CH	21	132.0	1H, *t*, *J* = 14.0 Hz	5.29	—	C-22
CH	22	127.5	1H, *d*, *J* = 12.7 Hz	5.33	—	C-17
CH_2	23	24.7	2H, *m*	1.53	—	—
CH_3	24	12.2	3H, *t*, *J* = 4.2 Hz	0.80	—	—
CH_3	25	19.7	3H, *s*	1.32	—	C-10
CH_2	26	29.8	2H, *d*, *J* = 3.7 Hz	1.25	—	C-14,27
CH_3	27	11.8	3H, *t*, *J* = 4.9 Hz	0.78	—	—
CH_2	28	65.7	2H, *s*	3.60	—	C-1′
CH_2	29	29.1	2H, *m*	1.52	H-30	—
CH_3	30	13.1	3H, *t*, *J* = 5.0 Hz	0.82	—	C-20
C	1′	179.4	—	—	—	—

Type	C. No.	^{13}C NMR	^{1}H. No. (int., mult., *J* in Hz)[b]	^{1}H NMR	COSY	HMBC
CH_2	15	29.4	1H, *dt*, *J* = 10.9, 6.3 Hz	1.59	—	C-14,16
			1H, d*t*, *J* = 11.9, 5.9 Hz	1.35	—	—
CH_2	16	37.0	1H, *dt*, *J* = 10.9, 5.9 Hz	1.60	—	C-17
			1H, *dt*, *J* = 11.2, 4.9 Hz	1.38	—	—
C	17	33.4	—	—	—	—
CH	18	41.4	1H, m	1.62	H-19	C-17
CH_2	19	37.7	1H, *t*, *J* = 4.9 Hz	1.20	—	C-20
			1H, *t*, *J* = 4.0 Hz	1.43	—	—
C	20	28.0	—	—	—	—
CH_2	21	33.9	1H, *dt*, *J* = 11.0, 4.8 Hz	1.61	—	C-20
			1H, *dt*, *J* = 10.0, 4.0 Hz	1.34	—	—
CH_2	22	34.3	1H, dt, *J* = 10.9, 4.7 Hz	1.56	—	C-21,17
			1H, *dt*, *J* = 10.5, 4.0 Hz	1.36	—	—
CH_2	23	19.1	2H, *q*, *J* = 5.7 Hz	2.13	—	C-4
CH_3	24	19.9	3H, *t*, *J* = 6.9 Hz	1.06	—	C-23
CH_3	25	20.8	3H, *s*	1.33	—	C-10,5
CH_3	26	19.7	3H, *s*	1.04	—	C-8
CH_3	27	19.4	3H, *s*	1.08	—	C-14

Table 1 (continued)

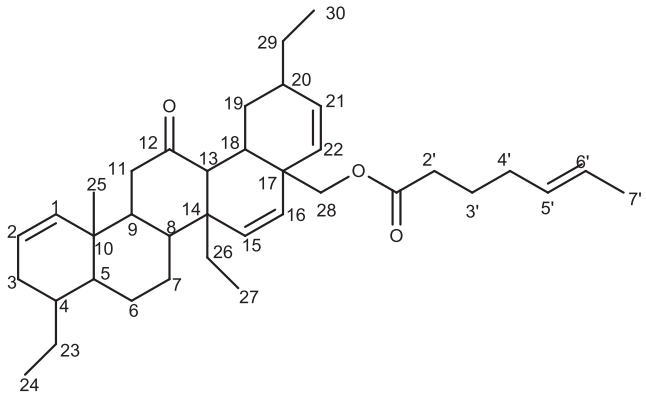

1

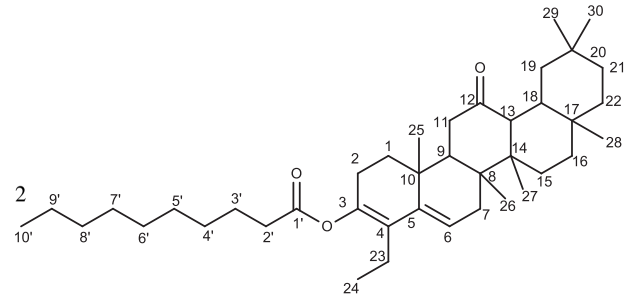

2

1

Type	C. No.	^{13}C NMR	^{1}H. No. (int., mult., J in Hz)[b]	^{1}H NMR	COSY	HMBC
CH_2	2′	25.6	2H, *t*, $J = 4.7$ Hz	1.63	H-3′	C-4′
CH_2	3′	26.9	2H, *m*	1.58	H-4′	C-2′
CH_2	4′	33.2	2H, *m*	2.20	H-5′	—
CH	5′	129.7	1H, *dt*, $J = 11.7$ Hz	5.26	—	—
CH	6′	128.0	1H, *m*	5.27	H-7′	C-5′
CH_3	7′	14.2	3H, *d*, $J = 9.2$ Hz	2.05	—	—
—	—	—	—	—	—	—
—	—	—	—	—	—	—
—	—	—	—	—	—	—
—	—	—	—	—	—	—
—	—	—	—	—	—	—
—	—	—	—	—	—	—
—	—	—	—	—	—	—

Type	C. No.	^{13}C NMR	^{1}H. No. (int., mult., J in Hz)[b]	^{1}H NMR	COSY	HMBC
CH_3	28	22.8	3H, *s*	1.10	—	C-17
CH_3	29	30.2	3H, *s*	0.88	—	C-20
CH_3	30	30.1	3H, *s*	0.96	—	C-20
C	1′	176.1	—	—	—	—
CH_2	2′	26.7	2H, t, $J = 10.9$ Hz	2.34	H-3′	C-1′
CH_2	3′	26.4	2H, *m*	1.63	H-4′	—
CH_2	4′	29.2	2H, *m*	1.29	H-5′	—
CH_2	5′	29.5	2H, *m*	1.23	H-6′	—
CH_2	6′	29.6	2H, *m*	1.28	H-7′	—
CH_2	7′	29.3	2H, *m*	1.32	H-8′	—
CH_2	8′	31.8	2H, *m*	1.30	H-9′	—
CH_2	9′	22.6	2H, *m*	1.31	H-10′	—
CH_3	10′	14.0	3H, *t*, $J = 7.3$ Hz	0.84	—	—

[a]NMR spectra were recorded using a Bruker AVANCE III 500 MHz (AV 500) spectrometer (Bruker, Karlsruhe, Germany) in $CDCl_3$ as aprotic solvent at ambient temperature with TMS as the internal standard (δ 0 ppm)

[b]Values in ppm, multiplicity and coupling constants (J = Hz) were indicated in parentheses. Multiplicities were allocated by ^{135}DEPT NMR spectrum

The assignments were made with the aid of the COSY, HSQC, HMBC and NOESY experiments

silica gel column resulted in eleven fractions (TA_1-TA_{11}). The percentage yield obtained for TA_2 (29%) were compared, and were found to be significantly greater than TA_1, TA_3 through TA_{11} (<15%, $P < 0.05$). The sub column fraction, TA_2 demonstrated greater antioxidative activities against free radicals, $ABTS^+$ (IC_{50} 0.6–1.0 mg mL^{-1}) and DPPH (IC_{50} 0.6–0.8 mg mL^{-1}) than other fractions ($IC_{50\ DPPH/ABTS^+} > 1.20$ mg mL^{-1}). Potential inhibitory activity towards starch digestive enzymes, α-glucosidase and α-amylase were characterised by the column sub-fractions, TA_2 ($IC_{50} < 0.25$ mg mL^{-1}), whereas the inhibition potentials of TA_1 and TA_3-TA_{11} were significantly lesser ($IC_{50} > 0.5$ mg mL^{-1}, $P < 0.05$). Therefore, the fraction, TA_2 was selected for further repeated chromatographic fractionations to yield two oleanene derivatives (**1**–**2**).

Spectroscopic characterisation

Two oleanene derivatives characterised as 24(4 → 23), 27(8 → 26), 30(20 → 29)-tris-abeo-olean-(12-oxo)-1,15,22-triene-methyl hept-5-enoate (**1**) and 24(4 → 23)-abeo-olean-(12-oxo)-3,5-diene-deconoate (**2**) were resulted from the repeated chromatographic fractionation of crude extract (EtOAc:MeOH) of *G. salicornia* (Fig. 1). The compounds were identified using comprehensive spectroscopic (mass spectroscopy, one and two-dimensional NMR, IR) analyses.

24(4 → 23), 27(8 → 26), 30(20 → 29)-Tris-abeo-olean-(12-oxo)-1,15,22-triene-methyl hept-5-enoate (1)

Repeated column chromatographic fractionation of *G. salicornia* yielded compound **1** as an yellow oily substance, which was characterised as 24(4 → 23), 27(8 → 26), 30 (20 → 29)-tris-abeo-olean-(12-oxo)-1,15,22-triene-methyl hept-5-enoate (**1**). The EI-MS experiment displayed the molecular ion peak at *m/z* 546, which along with NMR-IR spectroscopic analyses deduced its molecular formula as $C_{37}H_{54}O_3$ (Table 1). The FTIR signals at 1730 and 1726 cm^{-1} attributed the probable existence of ester and carbonyl functionalities, respectively. The ^{1}H NMR spectrum illustrated the occurrence of six deshielded olefinic hydrogens at δ_H5.32, δ_H5.28, δ_H5.34, δ_H5.30, δ_H5.29, δ_H5.33, δ_H5.26, and δ_H5.27. In addition, the shielded methyls (appeared as triplets) at δ_H0.80, δ_H0.78 and δ_H0.82 suggested the presence of methyl substitutions on triterpenoid system. The ^{13}C NMR along with ^{135}DEPT spectrum of **1** disclosed 37 carbon traces, encompassing five methyls (δ_C12.2, δ_C11.8, δ_C19.7, δ_C13.1, δ_C14.2), twelve sp^3 methylenes (δ_C31.8, δ_C29.0, δ_C28.9, δ_C39.3, δ_C31.7, δ_C24.7, δ_C29.8, δ_C65.7, δ_C29.1, δ_C25.6, δ_C26.9, δ_C33.2), eight sp^2 methines (δ_C130.2, δ_C127.8, δ_C130.5, δ_C127.7, δ_C132.0, δ_C127.5, δ_C129.7, 128.0), seven sp^3 methines (δ_C33.9, δ_C52.3, δ_C29.7, δ_C47.9, δ_C56.7, δ_C31.9, δ_C37.2), and five quaternary carbons (δ_C46.8, δ_C34.4, δ_C43.5), including two carbonyls (δ_C193.7, δ_C 179.4). The intense ^{1}H-^{1}H COSY spectrum of **1** demonstrated the occurrence of spin networks between (CH-δ_H5.28) (arbitrarily assigned as H-2)-(CH_2-δ_H1.77) (H-3)-(CH-δ_H1.62) (H-4)-(CH-δ_H1.30) (H-5)-(CH_2-δ_H1.51) (H-6)-(CH_2-δ_H1.26) (H-7)-(CH-δ_H1.33) (H-8)-(CH-δ_H1.66) (H-9)-(CH_2-δ_H2.22) (H-11) and (CH_2-δ_H1.65) (H-19)-(CH-δ_H1.93) (H-20)-(CH-δ_H5.29) (H-21), which supported the partial skeleton of pentacyclic ring in the triterpenoid (Fig. 2). The HMBC interactions from CH-1 (δ_H5.32) to CH-2 (δ_C127.8) and C-10 (δ_C46.8) determined the occurrence of olefinic bond at C-1 (δ_H5.32/δ_C130.2) and C-2 (δ_H5.28/δ_C127.8). The HMBC interactions between CH-15 (δ_H5.34) to C-14 (δ_C34.4) and those from CH-16 (δ_H5.30) to C-15 (δ_C130.5), C-17 (δ_C43.5) assigned an olefinic bond at C-15 (δ_H5.34/δ_C130.5) and C-16 (δ_H5.30/δ_C127.7). Likewise, HMBCs from CH-20 (δ_H1.93) and CH-21 (δ_H5.29) to C-22 (δ_C127.5) and from CH-22 (δ_H5.33) to C-17 (δ_C43.5) ascribed the occurrence of an olefinic bond between CH-21 (δ_H5.29/δ_C132.0) and CH-22 (δ_H5.33/δ_C127.5). This attribution was in agreement with the presence of olefinic bond in the E-ring system (Maneesh and Chakraborty 2017). Other HMBC correlations from CH-5

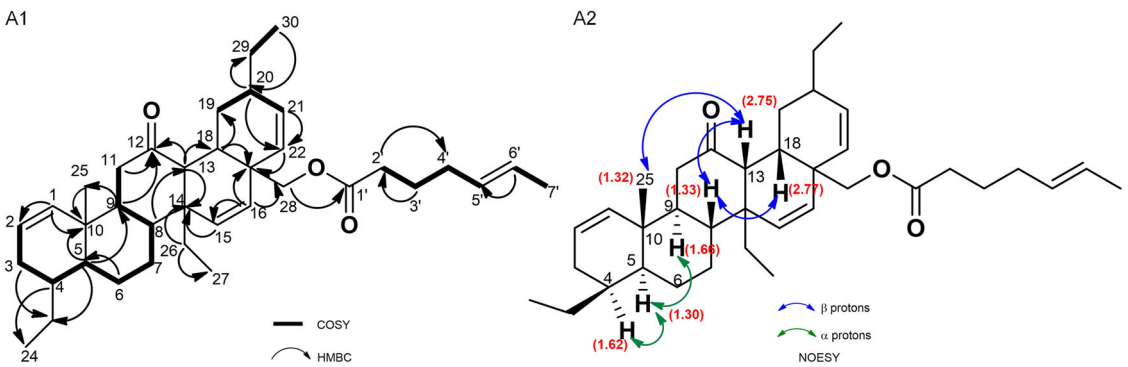

Fig. 2 (**A1**) ^{1}H-^{1}H COSY (bold-face bonds), selected HMBC (double-barbed arrows) and (**A2**) NOE (coloured arrows) correlations of 24(4 → 23), 27(8 → 26), 30(20 → 29)-tris-abeo-olean-(12-oxo)-1,15,22-triene-methyl hept-5-enoate (**1**) isolated from *G. salicornia*

(δ_H1.30) to C-10 (δ_C46.8), C-9 (δ_C47.9); from CH_2-6 (δ_H1.51) to C-5 (δ_C52.3); from CH-8 (δ_H1.33) to C-13 (δ_C56.7); CH-13 (δ_H2.75) to C-18 (δ_C31.9), C-14 (δ_C34.4) and from CH-18 (δ_H2.77) to C-19 (δ_C31.7), C-17 (δ_C43.5) were persistent with the pentacyclic skeleton of triterpenoid, **1**. The long range couplings from CH-9 (δ_H1.66), CH-13 (δ_H2.75) and CH_2-11 (δ_H2.22) to C-12 (δ_C193.7) revealed the C-12 keto functionality in **1**. This was comparable with the previously reported compound, dihydroxyolean-12-one, in which the chemical shift of C-12 was found to be δ_C208 due to the presence of neighbouring hydroxyl group at C-11 (δ_C71.8) (Da Rocha et al. 2015). No electronegative functionalities were apparent adjacent to keto group at C-12, hence it recorded lower chemical shift value in the present compound. These NMR assignments together with earlier reported values (Da Rocha et al. 2015; Huang et al. 2013; Maneesh and Chakraborty 2017) substantiated the presence of pentacyclic triterpenoid bearing olean-(12-oxo)-1,15,22-triene framework. The typical oleanene skeleton enclosed seven tertiary methyls in the range of δ_H0.7 to δ_H1.25 at C-4, C-10, C-8, C-14, C-17 and C-20 positions (Da Rocha et al. 2015; Maneesh and Chakraborty 2017), whereas the titled compound comprised of only one tertiary methyl at C-10. The position of tertiary methyl (CH_3-25) at C-10 was ascertained through the HMBCs from CH-9 (δ_H1.66) to CH_3-25 (δ_C19.7) and CH_3-25 (δ_C19.7) to C-10 (δ_C46.8), which was comparable with the earlier reports (Da Rocha et al. 2015). The angular methyl at C-4 (CH_3-24) in the basic oleanene framework was shifted to C-23, which was affirmed by the HMBC connections from CH_2-3 (δ_H1.77) to CH_2-23 (δ_C24.7); CH-4 (δ_H1.62) to CH_3-24 (δ_C12.2) and CH-5 (δ_H1.30) to CH_2-23 (δ_C24.7). The methyl at C-8 (CH_3-27) was shifted to C-26, which was corroborated by the HMBCs from CH_2-26 (δ_H1.25) to CH_3-27 (δ_C11.8), C-14 (δ_C34.4) (Fig. 2). Similarly, one of the *gem* dimethyl groups at C-20 (CH_3-30) was shifted to C-29, and was confirmed through the HMBC couplings from CH_3-30 (δ_H0.82) to CH-20 (δ_C37.2) and COSY couplings from (CH_2-δ_H1.52) (H-29)-(CH_3-δ_H0.82) (H-30). Therefore, the titled compound was classified as tris-abeo-oleanene triterpenoid, **1** which was named as 24(4 → 23), 27(8 → 26), 30(20 → 29)-tris-abeo-olean-(12-oxo)-triene. The typical angular methyl at C-17 (CH_3-28) was found to be deshielded in the present compound when compared to the previously reported chemical shift values (CH_3-28, δ_C28.43/δ_H 0.84) (Da Rocha et al. 2015), which was found to be δ_C65.7/ δ_H 3.60 (CH_2-28). This higher chemical shift was typical for the oxygenated protons, and its HMBC coupling to δ_C179.4 (C-1′) along with HMBC from CH-16 (δ_H5.30) to CH_2-28 (δ_C65.7) suggested the presence of an ester linkage in which oxygen was directly bonded to the sp^3 methylene at δ_H 3.60. The spin systems from (CH_2-δ_H1.63) (arbitrarily assigned as H-2′)-(CH_2-δ_H1.58) (H-3′)-(CH_2-δ_H2.20) (H-4′)-(CH-δ_H5.26) (H-5′) and (CH-δ_H5.27) (H-6′)-(CH_3-δ_H2.05) (H-7′) along with HMBCs from CH_2-2′ (δ_H1.63) to CH_2-4′ (δ_C33.2); CH_2-3′ (δ_H1.58) to CH_2-2′ (δ_C25.6) and CH-6′ (δ_H5.27) to CH-5′ (δ_C129.7) appropriately supported the presence of methyl hept-5-enoate chain at C-17. The titled compound was structurally related to previously reported oleanenes (Da Rocha et al. 2015; Huang et al. 2013; Maneesh and Chakraborty 2017; Oramas-Royo et al. 2010) besides the dissimilarities recognised in the positions of alkenes, tertiary methyls, ester linkages along with absence of hydroxyl functionalities. The relative stereochemistry of the chiral centres at δ_C33.9 (C-4), 52.3 (C-5), 29.7 (C-8), 47.9 (C-9), 56.7 (C-13), 31.9 (C-18) and 37.2 (C-20) were deduced from nuclear overhauser effect spectroscopy (NOESY) (Fig. 2). The proton at chiral centre, δ_H1.62 (assigned as CH-4) exhibited NOE with the proton (angular methyl) at δ_H1.30 (H-5) that were α-aligned (Wang et al. 2014). The α-disposition of protons at H-4, H-5, H-9 and H-20 were inferred by the NOE correlations between H-5 (δ_H1.30)/H-9 (δ_H1.66) and H-9 (δ_H1.66)/H-20 (δ_H1.93). On the contrary, the protons at δ_H1.32 (H-25), δ_H2.75 (H-13), δ_H1.33 (H-8), and δ_H2.77 (H-18) were positioned at the β-surface of reference plane, which were inferred by NOE correlations between H-25 (δ_H1.32)/H-13 (δ_H2.75), H-8 (δ_H1.33)/H-18 (δ_H2.77) and H-8 (δ_H1.33)/H-13 (δ_H2.75), The *trans*- and *cis*-intersection of ABCD and DE parts were reinforced by their stereochemical attributions (Koay et al. 2013). The structural elucidation of **1** was corroborated by the mass spectral experiment wherein the molecular ion at *m/z* 546.4 (1a) experienced the exclusion of methyl-hept-5-enoate to result 24(4 → 23), 27(8 → 26), 30(20 → 29)-tris-abeo-olean-(12-oxo)-1,15,22-triene (1b, *m/z* 419.3). The latter along with 1a underwent retro-Diels-Alder (rDA) rearrangement yielding the fragments *m/z* 126.1 (1c), 176.2 (1g), and 328.2 (1k). The spectroscopic experiments along with previous reports of literature unambiguously constructed of complete framework of oleanene triterpenoid, 24(4 → 23), 27(8 → 26), 30(20 → 29)-tris-abeo-olean-(12-oxo)-1,15,22-triene-methyl hept-5-enoate (**1**). The ion peak at *m/z* 176.2 (1g) was considered as the base peak (Fig. S12). These analyses suggested its molecular formula as $C_{37}H_{54}O_3$ enclosing eleven indices of hydrogen deficiencies associated with six olefinic bonds (comprising four alkenes and two carbonyls) and five ring systems. The spectroscopic experiments along with previous reports of literature unambiguously constructed of complete framework of oleanene triterpenoid, 24(4 → 23), 27(8 → 26), 30(20 → 29)-tris-abeo-olean-(12-oxo)-1,15,22-triene-methyl hept-5-enoate (**1**).

24(4 → 23)-Abeo-olean-(12-oxo)-3,5-diene-deconoate (2)

Repeated column chromatographic purification of the crude of *G. salicornia* isolated compound **2** as yellowish oily,

which was characterised as 24(4 → 23)-abeo-olean-(12-oxo)-3,5-diene-deconoate (**2**). The EI-MS spectrum displayed the molecular ion peak at *m/z* 592 along with NMR/IR analyses, which deduced its molecular formula as $C_{40}H_{64}O_3$ (Table 1). The FTIR vibrations at 1734 and 1634 cm^{-1} recognised the existence of ester and carbonyl functionalities, respectively. The ^{13}C NMR along with $^{135}DEPT$ spectrum of **2** displayed the presence of forty carbon signals, including eight methyl groups (δ_C19.9, δ_C20.8, δ_C19.7, δ_C19.4, δ_C22.8, δ_C30.2, δ_C14.0), eighteen sp^3 methylenes (δ_C30.5, δ_C24.7, δ_C34.0, δ_C36.9, δ_C29.4, δ_C37.0, δ_C37.7, δ_C33.9, δ_C34.3, δ_C19.1, δ_C26.7, δ_C26.4, δ_C29.2, δ_C29.5, δ_C29.6, δ_C29.3, δ_C31.8, δ_C22.6), one sp^2 methine (δ_C130.9), three sp^3 methines (δ_C43.4, δ_C51.9, δ_C41.4), and ten quaternary carbons (δ_C128.8, δ_C132.2, δ_C139.2, δ_C42.7, δ_C31.4, δ_C38.8, δ_C33.4, δ_C28.0) including two carbonyl carbons (δ_C213.1, δ_C176.1). The presence of one olefinic hydrogen was apparent at δ_H5.82, which exhibited HSQC correlation with δ_C130.9. The ^1H-^1H COSY experiment put forward the occurrence of three spin networks, which were found to be (CH_2-δ_H1.42) (arbitrarily assigned as H-1)-(CH_2-δ_H2.03) (H-2); (CH-δ_H1.70) (H-9)-(CH_2-δ_H2.33) (H-11) and (CH-δ_H2.30) (H-13)-(CH-δ_H1.62) (H-18)-(CH_2-δ_H1.20) (H-19) suggesting the partial fragments of pentacyclic ring in the triterpenoid (Fig. 3). The HMBC interactions from CH_2-2 (δ_H2.03) to C-4 (δ_C128.8), C-3 (δ_C132.2) determined the occurrence of tetrasubstituted olefinic bond at C-3 (δ_C132.2) and C-4 (δ_C128.8) and HMBCs from CH-6 (δ_H5.82) to C-5 (δ_C139.2), C-7 (δ_C34.0) attributed a trisubstituted olefinic bond at C-5 (δ_C139.2) and C-6 (δ_H5.82/δ_C130.9) (Fig. 3). Other HMBC correlations from CH_2-1 (δ_H1.42) to C-10 (δ_C31.4), C-5 (139.2); CH_2-2 (δ_H2.03) to C-1 (δ_C30.5); CH_2-7 (δ_H2.00) to C-8 (δ_C42.7); CH-9 (δ_H1.70) to C-8 (δ_C42.7), C-10 (δ_C31.4), C-11 (δ_C36.9); CH-13 (δ_H2.30) to C-8 (δ_C42.7) and C-14 (δ_C38.8); CH_2-15 (δ_H1.59) to C-14 (δ_C38.8) and C-16 (δ_C37.0); CH_2-16 (δ_H1.60) to C-17 (δ_C33.4); CH-18 (δ_H1.62) to C-17 (δ_C33.4); CH_2-19 (δ_H1.20) to C-17 (δ_C33.4); CH_2-21 (δ_H 1.61) to C-20 (δ_C 28.0) and CH_2-22 (δ_H1.56) to C-21 (δ_C33.9) appropriately supported the complete structure of pentacyclic triterpenoid, **2**. The long range couplings from both CH_2-11 (δ_H2.33) and CH-13 (δ_H2.30) to C-12 (δ_C213.1) deduced the C-12 keto functionality in **2**, whereas the attributions were comparable with the previously reported compound, trihydroxyolean-12-one in which the chemical shift of C-12 was found to be δ_C212 (Da Rocha et al. 2015). These NMR assignments in comparison with earlier reported chemical shift values (Da Rocha et al. 2015; Maneesh and Chakraborty 2017), which substantiated the presence of pentacyclic triterpenoid bearing olean-(12-oxo)-3,5-diene skeleton. The distinctive oleanene framework comprised of seven angular methyls in the δ_H0.7 to δ_H1.25 range at C-4 (CH_3-23, CH_3-24), C-10 (CH_3-25), C-8 (CH_3-26), C-14 (CH_3-27), C-17 (CH_3-28) and C-20 (CH_3-29, CH_3-30) positions (Da Rocha et al. 2015; Maneesh and Chakraborty 2017), whereas the titled compound comprised of six tertiary methyls at δ_H1.33 (s), δ_H1.04(s), δ_H1.08 (s), δ_H1.10 (s), δ_H0.88 (s) and δ_H0.96 (s). The position of tertiary methyl, δ_H1.33 (s) (CH_3-25) at C-10 was ascertained through HMBCs from δ_H1.33 to δ_C31.4 (C-10), δ_C139.2(C-5) and the HMBC correlations between δ_H1.04 to δ_C42.7 (C-8), which suggested the position of tertiary methyl, δ_H1.04 (s) (CH_3-26) at C-8. Similary, the HMBC couplings from δ_H 1.08 to δ_C38.8 (C-14) and that from δ_H1.10 (CH_3-28) to δ_C33.4 (C-17) confirmed the presence of angular methyl substitutions of CH_3-27 at C-14 and CH_3-28 at C-17, respectively. The *gem* dimethyls (CH_3-29, CH_3-30) at C-20 was confirmed by the long range relations of δ_H0.88 and 0.96 to δ_C28.0 (C-20). These six typical angular methyls were comparable with earlier reported chemical shifts of basic oleanene skelton (Da Rocha et al. 2015; Hassan et al. 2012). One of the *gem* dimethyl groups at C-4 (CH_3-24) was shifted to C-23, and this assignment was corroborated through the HMBC couplings from CH_2-23 (δ_H2.13) to C-4 (δ_C128.8) and CH_3-24 (δ_C1.06) to C-23 (δ_C19.1). Due to the methyl shift at C-4, the titled compound was classified as abeo-oleanene triterpenoid, **2** that was named as 24(4 → 23)-abeo-olean-(12-oxo)-3,5-diene. The COSY spin systems (CH_2-δ_H2.34)

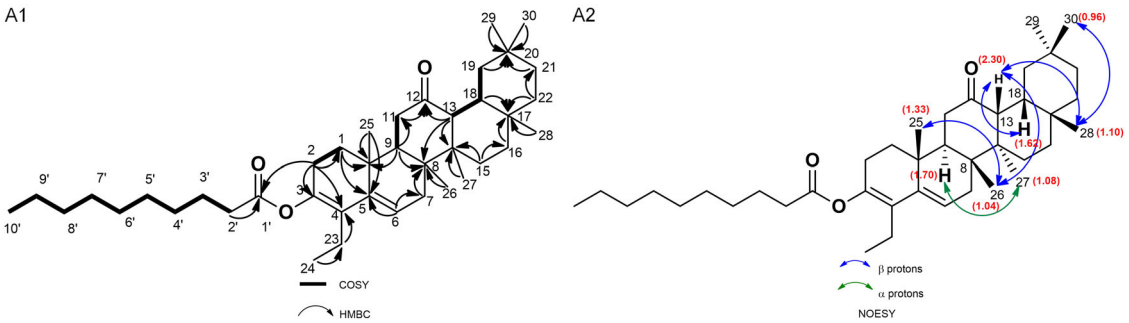

Fig. 3 (**A1**) ^1H-^1H COSY (bold-face bonds), selected HMBC (double-barbed arrows) and (**A2**) NOE (coloured arrows) correlations of 24(4 → 23)-abeo-olean-(12-oxo)-3,5-diene-deconoate (**2**) isolated from *G. salicornia*

(H-2′)-(CH_2-δ_H1.63) (H-3′)-(CH_2-δ_H1.29) (H-4′)-(CH_2-δ_H1.23) (H-5′)-(CH-δ_H1.28) (H-6′)-(CH_2-δ_H1.32) (H-7′)-(CH_2-δ_H1.30) (H-8′)-(CH_2-δ_H1.31) (H-9′)-(CH_3-δ_H0.84) (H-10′) attributed the presence of a linear side chain with nine carbon atoms. The HMBCs from CH_2-2 (δ_H2.03) to C-1′ (δ_C176.1) and CH_2-2′ (δ_H2.34) to C-1′ (δ_C176.1) supported the presence of an ester linkage attached to the nine alkyl membered linear chain. The previuos reports of 3-(stearyloxy)olean-12-ene enclosed 18-membered alkyl ester group in which the chemical shift at CH-3 was found to be δ_C80.51/δ_H4.52, and that of the ester carbonyl at C-1′ was found to be δ_C173.55 (Da Rocha et al. 2015). Herein, the chemical shift of ester carbonyl at C-1′ was found to be δ_C176.1 and this increase in the chemical shift was due to the direct attachment of oxygen end of the ester carbonyl to an alkenic quarternary carbon at C-3. The compound, **2** was structurally correlated to previously reported oleanenes (Da Rocha et al. 2015; Huang et al. 2013; Maneesh and Chakraborty 2017) beside the differences recorded in the dispositions of alkenes, ester linkages and presence of abeo tertiary methyls along with absence of hydroxyl functionalities. The relative stereochemistry of chiral centres at δ_C43.4 (C-9), 51.9 (C-13) and 41.4 (C-18) were worked out by nuclear overhauser effect spectroscopic (NOESY) experiments. The proton at δ_H2.30 (assigned to CH-13) exhibited NOE correlation with the angular methyl proton at δ_H1.04 (H-26) and δ_H1.62 (H-18) (Fig. 3) that was positioned in the β-plane (Wang et al. 2014). In addition, the β-disposition of chiral protons H-18, H-25, H-26, H-28 and H-30 were inferred by the NOE association between H-25 (δ_H1.33)/H-26 (δ_H1.04), H-26 (δ_H1.04)/H-13(δ_H2.30), H-13 (δ_H2.30)/H-18 (δ_H1.62), H-18 (δ_H1.62)/H-28 (δ_H1.10) and H-28 (δ_H1.10)/H-30 (δ_H0.96). These assessments were in agreement with the alignments of methyl functionalities at C-10, C-8 and C-20, as described in the previous reports of literature (Wang et al. 2014). Conversely, the proton at the chiral centre, δ_H1.70 (assigned as CH-9) exhibited NOE correlation with the proton at δ_H0.88 (H-29) that was disposed in the α-face. The other proton at δ_H1.08 (H-27) was found to be α-aligned. The *trans*-, *cis*-coincidence of ABCD and DE skeletons were substantiated by stereochemical attributions (Koay et al. 2013). The structural elucidation of **2** was corroborated by the mass spectral data wherein the molecular ion (*m/z* 592.5, 2a) experienced the exclusion of 2c to yield abeo-24(4 → 23)-olean-(12-oxo)-3,5-diene (2b) with *m/z* 421.3. The fragment, 1a underwent retro-Diels-Alder (rDA) rearrangement to afford the mass fragments 2 h and 2i (*m/z* 186.1 and 191.2, respectively). The ion peak at *m/z* 186.1 (2 h) was considered as the base peak (Fig. S24). These analyses deduced its molecular formula as $C_{40}H_{64}O_3$ enclosing nine indices of hydrogen deficiencies, which were associated with five ring systems and four olefinic bonds (comprising two carbonyls and two alkenes). The spectroscopic experiments along with previous reports of literature unambiguously characterised the oleanene triterpenoid as 24(4 → 23)-abeo-olean-(12-oxo)-3,5-diene-deconoate (**2**).

Bioactivities of abeo-oleanene terpenoids from *G. salicornia*

The in vitro anti-diabetic potential of the studied abeo-oleanenes (**1** and **2**) were assessed by their inhibitory properties towards the carbolytics, α-glucosidase and α-amylase that were found to regulate the intestinal carbohydrate absorption, thereby reducing postprandial insulin level (Goldstein et al. 1998). Among the titled abeo-oleanenes, the one with 24(4 → 23)-abeo-oleanene framework (**2**) displayed significantly higher α-amylase and α-glucosidase inhibitory properties (IC_{50} 0.32 and 0.29 mM, respectively) over that bearing 24(4 → 23), 27(8 → 26), 30 (20 → 29)-tris-abeo-oleanene moiety (**1**) (IC_{50} 0.40 and 0.34 mM, respectively) (Table 2). The higher α-amylase and α-glucosidase inhibitory properties of 24(4 → 23)-abeo-oleanene framework (**2**) (IC_{50} 0.32 and 0.29 mM, respectively) exhibited close resemblance towards the reference carbolytic enzyme inhibitor acarbose (IC_{50} 0.22 and 0.19 mM, respectively mM). In vitro radical scavenging assays by $ABTS^+$ and DPPH radicals were employed to deduce the antioxidant properties of studied abeo-oleanenes. The studied compound, **2** exhibited greater radical scavenging activities (IC_{50} DPPH 1.33 mM; IC_{50} $ABTS^+$ 1.09 mM), when compared to those displayed by compound **1** (IC_{50} DPPH 1.56 mM; IC_{50} $ABTS^+$ 1.24 mM) and standard, α-tocopherol (IC_{50} DPPH 1.46 mM; IC_{50} $ABTS^+$ 1.72 mM).

The target bioactivities of the studied compounds were assessed by different physicochemical parameters, and these were utilised to correlate their structural attributes. It is consequential to record that the electronic parameter of 24 (4 → 23)-abeo-oleanene (**2**) (Pl ~70×10^{-24} cm^3) was greater than that recorded with 24(4 → 23), 27(8 → 26), 30 (20 → 29)-tris-abeo-oleanene (**1**) (polarisability, Pl ~65×10^{-24} cm^3), which could substantiate the greater inhibitory activities of former towards oxidants and carbolytic enzymes. It was apparent that the compound **2** was bulkier than **1**, as determined by the greater steric factors of the former. Comparatively lesser bulkiness of **1** and **2** (MR 163–178 cm^3 mol^{-1}, MV 541–575 cm^3 mol^{-1} and Pr 1320–1445 cm^3) might efficiently network with the enzyme active site remnants, resulting in its higher inhibitory activity towards starch digestive enzymes (Table 3). It was also likely that that a greater hydrophobicity (logarithmic value of octanol-water coefficient) of abeo-oleanenes, **1**–**2** (log P_{ow} 9.19–10.73) predominantly contributed towards its greater radical quenching and carbolytic enzyme inhibitory activities. The higher hydrophobic values might explain its

Table 2 In vitro bioactive potentials (antioxidant and anti-diabetic)[a] of compounds **1–2** from *G. salicornia* and commercially available references

Bioactivities (IC_{50}, mM)			
Antioxidant activity	1	2	α-Tocopherol
DPPH scavenging activity	[b]1.56 ± 0.01	[c]1.33 ± 0.01	[d]1.46 ± 0.01
$ABTS^+$ scavenging activity	[b]1.24 ± 0.02	[c]1.09 ± 0.02	[d]1.72 ± 0.03
Anti-diabetic activity	1	2	Acarbose
α-amylase inhibition activity	[b]0.40 ± 0.01	[c]0.32 ± 0.02	[d]0.22 ± 0.02
α-glucosidase inhibition activity	[b]0.34 ± 0.01	[c]0.29 ± 0.03	[d]0.19 ± 0.01

[a]The antioxidant and anti-diabetic activities were expressed as IC_{50} values (mM)

[b–d]Row-wise values with different superscripts of this type indicate significant difference ($P < 0.05$), which implied for the statistical evaluation of the results. Triplicate values were taken and the variance analyses (ANOVA) were carried out (using Statistical Program for Social Sciences 13.0) for means of all parameters to examine the significance level ($P < 0.05$)

Results were expressed as mean ± SD ($n = 3$)

Table 3 Molecular descriptors (electronic, steric and hydrophobic) of compounds 1–2 from *G. salicornia*

Molecular descriptors		
	1	2
Electronic		
tPSA	43.37	43.37
Pl ($\times 10^{-24}$ cm^3)	64.99	70.61
Steric		
MR (cm^3 mol^{-1})	163.95	178.13
MV (cm^3 mol^{-1})	541.40	575.80
Pr (cm^3)	1320.60	1445.10
Hydrophobic		
Log P_{ow}	9.19	10.73

The structure-activity relationship analyses were carried out by using different molecular descriptors of the purified compounds as described in the text

MV molar volume, *Pr* parachor, *MR* molar refractivity, *Log* P_{ow} logarithmic scale of the octanol-water partition coefficient, *Pl* polarisability, *tPSA* topological polar surface area

requisite hydrophobic-hydrophilic interactions (Lipinski 2004) and bonding of receptor enzymes (Huuskonen et al. 2000) leading to its higher anti-hyperglycaemic and anti-oxidant properties.

Molecular docking analysis of the abeo-oleanenes isolated from *G. salicornia*

The inhibition of starch degrading enzymes, such as α-amylases and α-glucosidases is an effective methodology to monitor the glucose level in blood. The commercially developed carbolytic enzyme inhibitors, such as acarbose and voglibose are widely used to control the blood glucose levels. The computation tools like structure based molecular docking simulations have been widely utilised to enrich a chemical library of active compounds with biomolecular structure and functions (Hyun et al. 2014). The studied oleanene analogues were subjected to molecular docking studies against starch digestive enzymes, α-glucosidase and α-amylase. The results were evaluated by their RMSD data. The molecular docking parameters, such as binding energy, intermolecular and torsional free energy, and inhibition constants of **1–2** were documented (Table 4). In silico molecular docking analysis of the abeo-oleanenes with α-glucosidase with grid box $x = 37.969$, $y = -19.190$, $z = 29.008$ and α-amylase with grid box $x = -7.248$ $y = 54.607$, $z = 30.003$ appropriately gave the impression that the ligands exhibited efficient interactions with the enzyme target sites (Fig. 4). Among the studied oleanenes (**1–2**), compound **2** recorded least binding energy of -9.84 kcal mol^{-1} in interactions with α-glucosidase enzyme target sites subsequent to those exhibited by compound **1** (-9.42 kcal mol^{-1}). Likewise, the constant of enzyme inhibition (Ki) was lesser for **2** (61.61 nM) towards α-glucosidase enzyme than that exhibited by **1** (124.49 nM). Also, intermolecular energy was lesser for **2** (-11.44 kcal mol^{-1}). The molecular docking interaction of ligand (oleanene **2**) and α-glucosidase showed two hydrogen bonds (displayed as red-coloured lines) to amino acyl residues of THR^{83} and TRP^{36} with the bond distances of 3.148 and 3.044 Å in the active binding site, whereas **1** showed one hydrogen-bonded interaction to amino acid residue of TRP^{36} with molecular distance of 2.766 Å.

Similarly, compound **2** exhibited least binding energy of -10.04 kcal mol^{-1} in α-amylase enzyme target site interactions than those exhibited by compound **1** (-5.52 kcal mol^{-1}). Additionally, two other parameters, such as intermolecular energy and inhibition constant (Ki) were also calculated. The compound **2** had lesser inhibition constant (38.15 nM) when compared to **1** (89.58 µM). Inhibition constant and binding energy were proportional to each

Table 4 The binding energy, inhibition constant, intermolecular energy and torsional free energy between the ligands (compounds **1**–**2**) and the active sites of carbolytic enzymes α-glucosidase and α-amylase

[a]Ligands	[b]Binding energy (kcal mol^{-1})	[b]Inhibition constant, Ki (nM) (μM)	[b]Intermolecular energy (kcal mol^{-1})	[b]Torsional free energy (kcal mol^{-1})	Amino acid residue	Molecular distances
α-glucosidase						
1	−9.42	124.49	−11.14	1.79	TRP^{36}	2.766
2	−9.84	61.61	−11.44	2.39	THR^{83}, TRP^{36}	3.148, 3.044
α-amylase						
1	−5.52	89.58	−7.06	1.79	ASP^{381}	2.467
2	−10.04	38.15	−12.18	2.39	ARG^{346}	2.954, 2.878

[a]Molecular docking simulations were carried out using Autodock 4 software tool

[b]Values were evaluated from the calculations based on the energy minimisation

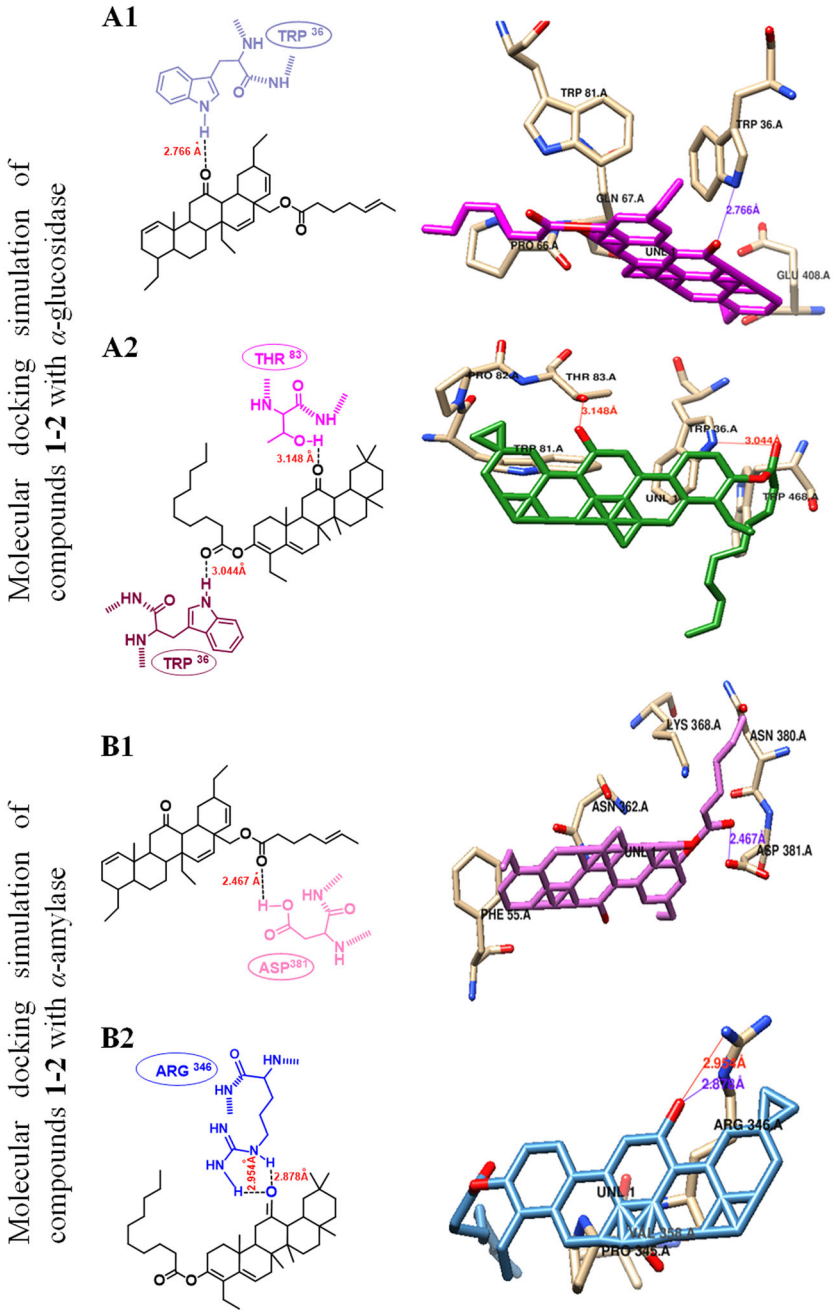

Fig. 4 Closer view of molecular binding interactions of (**A1**) 24(4 → 23), 27(8 → 26), 30(20 → 29)-tris-abeo-oleanene **1** and (**A2**) 24(4 → 23)-abeo-oleanene **2** derivatives in the catalytic site of protein α-glucosidase along with molecular-binding interactions of (**B1**) 24(4 → 23), 27(8 → 26), 30(20 → 29)-tris-abeo-oleanene **1** and (**B2**) 24(4 → 23)-abeo-oleanene **2** derivatives in the catalytic site of α-amylase as deduced from its molecular modelling simulations

other, and therefore, the inhibitory activity of α-amylase of **2** was substantiated by using intermolecular energy and inhibition constant. As mentioned in Table 4, the metabolite **2** exhibited intermolecular energy of $-12.18\,\text{kcal mol}^{-1}$, which was lesser when compared to **1** ($-7.06\,\text{kcal mol}^{-1}$). These results further demonstrated greater α-amylase inhibition activity of oleanene **2** compared to that exhibited by **1**. The molecular docking analysis of oleanene **2** and α-amylase showed two hydrogen bonds with amino acyl residue of ARG^{346} with the bond distances of 2.954 and 2.878 Å in the active binding site, whereas compound **1** showed one hydrogen-bonded interaction with amino acyl residue of ASP^{381} with molecular distance of 2.467 Å. The comparison of molecular docking parameters on the basis of in vitro experiment appropriately suggested that the abeo-oleanene derivative (**2**) exhibited closer molecular interactions with the starch digestive enzymes, which might explain its greater inhibitory potential against α-glucosidase and α-amylase (0.29–0.34 mM) when compared to those exhibited by **1** (0.32–0.40 mM). It was thus apparent that active inhibition of the pancreatic α-amylase enzyme could be an efficient approach to decrease the postprandial hyperglycaemic levels via regulation of carbohydrate breakdown.

The antioxidant potencies of oleanene-type triterpenoids through the DPPH radical scavenging mechanism were previously recorded (Ahmad et al. 2008) that could be correlated with the studied antioxidative oleanene triterpenoids. The hypoglycaemia activity of terpenoids and their potential to safeguard the β-cells were documented previously (Roth et al. 2002). The tris-abeo-oleanene (**1**) enclosed four olefinic groups, whereas two olefinic moieties were apparent in abeo-oleanene (**2**). Both the metabolites were found to constitute one each of ketone and ester functionalities, whereas these groups could participate in the effective electron delocalizations in DPPH scavenging mechanism, that might be one of the reasons for potent antioxidative effects of **1** and **2**. In the case of anti-diabetic potential, the titled oleanenes exhibited greater α-glucosidase inhibition than α-amylase inhibition, demonstrating the favoured α-glucosidase inhibition of seaweed-derived oleanene triterpenoids (Maneesh and Chakraborty 2017). Even though, the tris-abeo-oleanene, **1** enclosed greater number of unsaturations when compared to abeo-oleanene (**2**), the polarisability and hydrophobicity parameters were greater for **2**. However, the greater polarisability and hydrophobicity were found to be responsible for the bological potencies of **2** (Wang et al. 2007), and thus, it was suggested that electronegative groups alone were not responsible for its greater bioactivities. Similarly, greater hydrophobicity of **2** compared to **1** suggested a balanced hydrophobicity and hydrophilic characteristics of **2** desirable for the target biological properties. Thus, abeo-oleanene **2** with higher hydrophobicity (log P_{ow} 10.73) could play prominent role in greater carbolytic enzyme inhibitory acivities over that displayed by tris-abeo-oleanene, **1** with lower hydrophobicity (log P_{ow} 9.19). The in silico molecular docking studies of **1**–**2** with α-amylase and α-glucosidase enzyme exhibited binding interactions, and these results appropriately indicated that compound **2** displayed strong binding interactions with α-glucosidase and α-amylase compared to those exhibited by compound **1** (Fig. S25–S27). Thus, the 24(4 → 23)-abeo-oleanene triterpenoid bearing (12-oxo)-3,5-diene-deconoate moiety (compound **2**) derived from *G. salicornia*, might function as potential bioactive candidate in the development of anti-hyperglycaemic lead.

Conclusions

The organic extract of *G. salicornia* was fractionated by repeated chromatographic techniques to obtain two unprecedented abeo-oleanene analogues. Among the isolated compounds, the one with 24(4 → 23) abeo-oleanene framework (**2**) exhibited higher carbolytic enzyme inhibitory activities ($IC_{50} \le 0.32$ mM) over that bearing 24(4 → 23), 27 (8 → 26), 30(20 → 29)-tris-abeo-oleanene moiety (**1**) ($IC_{50} \ge 0.34$ mM). The oleanene analogues isolated from *G. salicornia* registered greater radical scavenging potentials against $ABTS^{+}$ ($IC_{50} < 1.10$ mM) than that exhibited by α-tocopherol ($IC_{50} > 1.50$ mM). Structure-activity relationship analyses showed that higher polarisability and lesser steric bulk of abeo-oleanene (**2**) predominantly contributed towards the comparatively greater radical quenching and carbolytic enzyme inhibitory activities than those displayed by its tris-abeo-oleanene analogue (**1**). In silico molecular modelling studies were performed to designate the α-glucosidase and α-amylase inhibitory mechanism of the abeo-oleanene derivative (**2**) exhibiting binding energies of greater than $9.50\,\text{kcal mol}^{-1}$, which substantiated its potential inhibitory activity against the carbolytic enzymes responsible to cause hyperglycaemic disorders. An enzyme-assisted putative biosynthetic cascade leading to the formation of oleanene triterpenoid derivatives were proposed. In particular, the 24(4 → 23)-abeo-oleanene possessing (12-oxo)-3,5-diene-deconoate moiety (compound **2**) was found to be effective dual inhibitors of starch digestive enzymes along with potential antioxidative properties, and therefore, might be utilised as valuable medicinal lead against oxidant species and elevated postprandial glucose levels.

Acknowledgements The present work was supported by Science and Engineering Research Board (SERB) (grant number SR/S1/OC-96A/2012) of Department of Science and Technology, New Delhi, India. The authors thank the Director, Indian Council of Agricultural Research-Central Marine Fisheries Research Institute (ICAR-CMFRI),

and Head, Marine Biotechnology Division, ICAR-CMFRI for guidance and support.

Compliance with ethical standards

Conflict of interest The authors declare that they have no conflict of interest.

Ethical approval This article does not contain any studies with human participants or animals performed by any of the authors.

Publisher's note: Springer Nature remains neutral with regard to jurisdictional claims in published maps and institutional affiliations.

References

Ahmad Z, Mehmood S, Fatima I, Malik A, Ifzal R, Afza N, Iqbal L, Latif M, Nizami TA (2008) Structural determination of salsolins A and B, new antioxidant polyoxygenated triterpenes from *Salsola baryosma* by 1D and 2D NMR spectroscopy. Magn Reson Chem 46:94–98

Antony T, Chakraborty K (2018) First report of antioxidant abeolabdane type diterpenoid from intertidal red seaweed *Gracilaria salicornia* with 5-lipoxygenase inhibitory potential. Nat Prod Res https://doi.org/10.1080/14786419.2018.1508150

Brayer GD, Luo Y, Withers SG (1995) The structure of human pancreatic alpha-amylase at 1.8 A resolution and comparisons with related enzymes. Protein Sci 4:1730–1742

Cen-Pacheco F, Nordstrom L, Souto ML, Martin MN, Fernandez JJ, Daranas AH (2010) Review: studies on polyethers produced by red algae. Mar Drugs 8:1178–1188

Da Rocha CQ, Vilela FC, Santa-Cecilia FV, Cavalcante GP, Vilegas W, Giusti-Paiva A, Dos Santos MH (2015) Oleanane-type triterpenoid: an anti-inflammatory compound of the roots *Arrabidaea brachypoda*. Rev Bras Farmacogn 25:228–232

De Almeida CLF, Falcao HDF, Lima GRDM, Montenegro CDA, Lira NS, de Athayde-Filho PF, Rodrigues LC, de Souza MDFV, Barbosa-Filho JM, Batista LM (2011) Bioactivities from marine algae of the genus *Gracilaria*. Int J Mol Sci 12:4550–4573

Francavilla M, Franchi M, Monteleone M, Caroppo C (2013) The red seaweed *Gracilaria gracilis* as a multi products source. Mar Drugs 11:3754–3776

Goldstein BJ, Ahmad F, Ding W, Li PM, Zhang WR (1998) Regulation of the insulin signaling pathway by cellular protein-tyrosine phosphatases. Mol Cell Biol 182:91–99

Hamdan II, Afifi FU (2004) Studies on the in vitro and in vivo hypoglycemic activities of some medicinal plants used in treatment of diabetes in Jordanian traditional medicine. J Ethanopharmacol 93:117–121

Hassan EM, Mohammed MMD, Mohamed SM (2012) Two new phorbol-type diterpene esters from *Synadenium grantii* Hook F. leaves. Rec Nat Prod 6:255–262

Henriksen EJ, Diamond-Stanic MK, Marchionne EM (2011) Oxidative stress and the etiology of insulin resistance and type-2 diabetes. Free Radic Biol Med 51:993–999

Hill RA, Connolly JD (2012) Triterpenoids. Nat Prod Rep 29:780–818

Huang YL, Sachi N, Tanaka T, Matsuo Y, Saito Y, Kouno I (2013) Two new oleanane-type triterpenes isolated from Japanese post-fermented tea produced by anaerobic microbial fermentation. Molecules 18:4868–4875

Huuskonen JJ, Livingstone DJ, Tetko IV (2000) Neural network modelling for estimation of partition coefficient based on atom-type electrotopological state indices. J Chem Inf Comput Sci 40:947–955

Hyun TK, Eom SH, Kim J-S (2014) Molecular docking studies for discovery of plant-derived α-glucosidase inhibitors. POJ 7:166–170

Koay YC, Wong KC, Osman H, Eldeen IMS, Asmawi MZ (2013) Chemical constituents and biological activities of *Strobilanthes crispus* L. Rec Nat Prod 7:59–64

Kumar S, Narwal S, Kumar V, Prakash O (2011) α-Glucosidase inhibitor from plants: a natural approach to treat diabetes. Phcog Rev 5:19–29

Kwon YI, Apostolidis E, Kim YC, Shetty K (2007) Health benefits of traditional corn, beans and pumpkin: in vitro studies for hyperglycemia and hypertension management. J Med Food 10:266–275

Laszczyk MN (2009) Pentacyclic triterpenes of the lupane, oleanane and ursane group as tools in cancer therapy. Planta Med 75:1549–1560

Lee DY, Yang H, Kim HW, Sung SH (2017) New polyhydroxy triterpenoid derivatives from fruits of *Terminalia chebula* Retz and their α-glucosidase and α-amylase inhibitory activity. Bioorg Med Chem Lett 27:34–39

Lipinski CA (2004) Lead and drug-like compounds: the rule-of-five revolution. Drug Discov Today Technol 1:337–341

Maneesh A, Chakraborty K (2017) Previously undescribed fridooleanenes and oxygenated labdanes from the brown seaweed *Sargassum wightii* and their protein tyrosine phosphatase-1B inhibitory activity. Phytochem 144:19–32

Na M, Cui L, Min BS, Bae K, Yoo JK, Kim BY (2006) Protein tyrosine phosphatase-1B inhibitory activity of triterpenes isolated from *Astilbe koreana*. Bioorg Med Chem Lett 16:3273–3276

Nazaruk J, Borzym-Kluczyk M (2015) The role of triterpenes in the management of diabetes mellitus and its complications. Phytochem Rev 14:675–690

Perera PRD, Ekanayake S, Ranaweera KKDS (2013) In vitro study on antiglycation activity, antioxidant activity and phenolic content of *Osbeckia octandra* L. leaf decoction. J Pharmacogn. Phytochem 2:198–201

Roth BL, Baner K, Westkaemper R, Siebert D, Rice KC, Steinberg S, Ernsberger P, Rothman RB (2002) Salvinorin A: a potent naturally occurring non nitrogenous kappa opioid selective agonist. Proc Natl Acad Sci USA 99:11934–11939

Ruzicka L (1963) Perspectives of the biogenesis and chemistry of terpenes. Pure Appl Chem 6:493–522

Oramas-Royo SM, Chavez H, Martin-Rodriguez P, Fernandez-Perez L, Ravelo AG, Estevez-Braun A (2010) Cytotoxic triterpenoids from *Maytenus retusa*. J Nat Prod 73:2029–2034

Sasaki T, Li W, Morimura H, Li S, Li Q, Asada Y, Koike K (2011) Chemical constituents from *Sambucus adnata* and their protein-tyrosine phosphatase-1B inhibitory activities. Chem Pharm Bull 59:1396–1399

Sekar S, Viswanathan KP, Kishnan B, Ganesan KK (2015) Evaluation of anti-hyperglycemic effect of *Gracilaria corticata* extract in normal and streptozotocin-induced diabetic rats. Chem. Biol Lett 2:6–11

Tahrani AA, Bailey CJ, Del Prato S, Barnett AH (2011) Management of type 2 diabetes: new and future developments in treatment. Lancet 378:182–197

Wang J, Xie X-Q, Hou T, Xu X (2007) Fast approaches for molecular polarisability calculations. J Phys Chem A 111:4443–4448

Wang J, Xu QL, Zheng M-F, Ren H, Lei T, Wu P, Zhou ZY, Wei XY, Tan JW (2014) Bioactive 30-noroleanane triterpenes from the pericarps of *Akebia trifoliata*. Molecules 19:4301–4312

Wojdylo A, Oszmianski J, Czemerys R (2007) Antioxidant activity and phenolic compounds in 32 selected herbs. Food Chem 105:940–949

Wu C, Huang S, Yen GC (2011) Silymarin: a novel antioxidant with antiglycation and antiinflammatory properties *in vitro* and *in vivo*. Antioxid Redox Signal 14:353–366

Yamamoto K, Miyake H, Kusunoki M, Osaki S (2010) Crystal structures of isomaltase from *Saccharomyces cerevisiae* and in complex with its competitive inhibitor maltose. FEBS J 277:4205–4214